



## Power Generation and Desalination from an Abandoned Oil Well: Kalina Cycle-Driven Reverse Osmosis System

Mohammad Norouzi<sup>1,\*</sup> - Kianoosh Rezaie<sup>2</sup>

<sup>1</sup>Department of Chemical Engineering, Amirkabir University of Technology, Tehran, Iran

<sup>2</sup>Department of Environmental Engineering, College of Engineering, University of Tehran, Tehran, Iran

### ABSTRACT

*The sustainable production of potable water is inherently dependent on a stable and efficient energy source. This interdependence is crucial for fostering trust and investment from stakeholders across industries, research communities, and investors. This study presents an innovative approach, integrating geothermal energy—sourced from an abandoned oil well (AOW) in Iran, which eliminates drilling costs—with a Kalina Cycle System 11 (KC-11) power generation system and a reverse osmosis (RO) desalination unit. By leveraging geothermal energy, a clean, renewable, and virtually unlimited resource, this system aims to meet large-scale demands for both electricity and water. The KC-11 was simulated using EES software, revealing that the injection of geothermal fluid can generate 110 kWh of power efficiently at optimal pressure levels. Simultaneously, the RO unit, modeled with WAVE software, demonstrated that a power input of 4.87 kWh per 1 m<sup>3</sup> is sufficient to achieve the client's potable water requirement of 806 m<sup>3</sup>/day. The results underline the economic and operational benefits of utilizing AOW-derived geothermal energy, offering a sustainable and cost-effective model for integrated water and energy production that aligns with global environmental and resource efficiency goals.*

**Keywords:** Power Generation, Reverse Osmosis, Geothermal Energy, Desalination, Abandoned Oil Well, Kalina Cycle

### 1. INTRODUCTION

Access to drinking water and energy supply have become fundamental human needs for survival, yet obtaining them is not as simple as it may seem. Many regions around the world struggle with water scarcity, facing numerous challenges to secure even a drop of potable water. On the other hand, without a reliable supply of energy, whether in the form of electricity or heat, industries would come to a standstill, and darkness would engulf the world. Recognizing the critical importance of these resources, scientists and researchers have made significant efforts over the past years to address water and energy shortages and ensure a sustainable future for the next generation. While some solutions have been successfully implemented, others are still in the evaluation phase or facing certain obstacles. In the modern era, the focus on clean energy has emerged as the most promising solution. It holds the potential to provide a sustainable energy supply for both domestic use and large industries, including water purification. The availability of renewable energy resources varies by geographic region, but the diversity of these resources — such as solar, geothermal, wind, and biomass — means that virtually every part of the world has some advantage to harness. These resources offer a significant opportunity for policymakers to develop long-term solutions to both energy and water challenges [1-6].

Among renewable energy sources, geothermal energy holds particular significance due to its fewer limitations compared to others. It is a resource that operates independently of weather conditions and seasons, providing a constant capacity around the clock. A critical factor in geothermal energy is the geothermal gradient, which varies for each well. This gradient provides comprehensive data on the temperature at different depths and its variation throughout the well, serving as a key parameter in evaluating the capacity of a



geothermal well [7-12]. For instance, geothermal fluids with temperatures below  $100^{\circ}\text{C}$  can be applied in industries such as fish farming or localized heating. Temperatures between  $100^{\circ}\text{C}$  and  $150^{\circ}\text{C}$  can be used in medium-scale water purification industries, while temperatures exceeding  $150^{\circ}\text{C}$  are suitable for large-scale combined power and water production industries. Given that the focus of this paper is desalination, Figure 1 presents a schematic of geothermal energy applications in desalination processes [13-15].

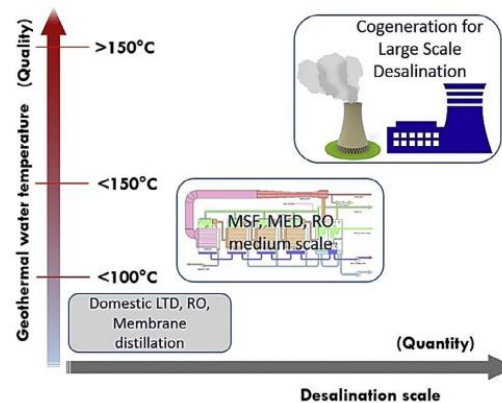


**Fig. 1.** Schematic representation of geothermal energy applications in desalination processes [14]

The primary challenge in utilizing geothermal energy, depending on the intended use, lies in the drilling process. Drilling challenges have hindered the broader evaluation of geothermal energy. However, a breakthrough solution has recently been discovered by researchers, which could reduce the investment cost by over 50%. This solution involves repurposing abandoned oil wells (AOW) as alternative geothermal sources. The widespread availability of these wells, especially in oil-rich countries, has significantly increased the appeal of geothermal energy as a viable option for energy production. In order to fully capitalize on the geothermal potential of AOW, it is imperative to explore innovative methods such as implementing power generation cycles. By leveraging this approach, we can effectively convert the existing resources into sustainable energy sources, thereby contributing to a more environmentally friendly and efficient energy landscape [18-22]

### 1.1 Literature Review

In a recent numerical simulation conducted by Rezaie et al. [23], they analyzed a cogeneration system that utilized a chemisorption power cycle. The results revealed that the system achieved a maximum electrical power output of 2.7 kW and a cooling capacity of 14.5 kW. In a recent study by Mehri et al. [24], a new method of using geothermal energy to generate electricity and pure water simultaneously was introduced. The proposed approach involves the utilization of a Kalina cycle (KC) and vaporization. The cycle has the capacity to produce up to 2.94 MW of electrical power and 0.34 kg/s of pure water. The geothermal water, with a mass flow rate of 89 kg/s and a temperature of  $124^{\circ}\text{C}$ , is used for the process.

A recent study investigated a cogeneration plant that combines power and pure water production using hybrid biomass and geothermal energies [25]. The proposed plant incorporates a gas turbine integrated with the Rankine Cycle (RC), leveraging geothermal energy to enhance the bottoming RC. Water desalination is achieved through reverse osmosis (RO), powered by the electricity generated from the bottoming cycle. The research findings demonstrated that under optimal conditions, the proposed plant exhibits significantly improved performance compared to its base case operation mode. The optimization process resulted in a 19.8% increase in power production and a 49.1% increase in pure water production. Additionally, the plant's exergetic efficiency increased by 6.85%. The study suggests that the proposed cogeneration plant can enhance the efficiency of power and pure water production, providing a sustainable and eco-friendly solution.

A proposed system integrates geothermal energy and parabolic trough solar collectors to simultaneously produce power, cooling, freshwater, hydrogen, and heat across multiple generations [26]. The system



harnesses a Steam Rankine Cycle (SRC) and an Organic Rankine Cycle (ORC) to generate power, while also producing hot water using a domestic water heater, generating hydrogen through proton exchange membrane (PEM) electrolysis, and creating freshwater alongside electricity generation. The system yields hydrogen at a mass flow rate of 2.648 kg/h, freshwater at a rate of 32.68 m<sup>3</sup>/h, a cooling load of 275.6 kJ/s, and hot domestic water at a rate of 13.36 kg/s.

Geothermal energy systems show promise as a renewable energy source, but the drilling process required to harness this energy can be prohibitively expensive. As a result, researchers have been exploring alternative options, with one promising avenue being the repurposing of abandoned oil wells (AOW). With millions of such wells scattered around the world, they represent a vast potential source of geothermal energy. Initial evaluations have shown that repurposing these wells can significantly reduce the costs associated with developing geothermal energy systems. Noorollahi et al. [27] conducted a project aimed at generating electricity from a binary cycle powered by a geothermal AOW located in the Ahwaz oil field in Iran. To achieve this, the team designed a coaxial borehole heat exchanger (CBHE) that would inject water as the working fluid into the well. Subsequently, the water would receive heat from the well depth and be extracted as hot liquid water that could be utilized for a power generation binary cycle. Following the simulation of the project, Noorollahi et al. [28] discovered that the oil field with a bottom-hole temperature of 159.8 °C has the potential to generate an impressive 364 kW of electricity. The results of the project demonstrate the potential for the conversion of AOW into productive geothermal energy sources, providing a sustainable and environmentally friendly source of electricity.

Norouzi et al. [22] made several improvements to the AOW system. They used advanced techniques like the  $k-\omega$  SST turbulence model and the mapped meshing method. They also added nano thermal-insulation along the well to reduce heat loss, resulting in a 7% increase in the extracted water temperature. They then studied a modified multi-effect distillation (MED) system and found that a 12-effect MED system with flash boxes increased fresh water production by approximately 33%.

Our research is focused on harnessing thermal energy extracted from an AOW as a sustainable geothermal heat source. This energy will be utilized to power a plant known as KC and facilitate the production of potable water through an RO system. The power generation cycle was meticulously simulated using the Engineering Equation Solver (EES) software. Additionally, we utilized the Wave software to precisely calculate the volume of water generated through the reverse osmosis process.

## 2. METHODOLOGY

### 2.1 Case Study

A ground heat exchanger must be designed to use the AOW located in the Ahwaz oil field [22], as indicated in Figure 2. When it comes to ground heat exchangers, the CBHE stands out as the optimal choice for enhancing both technical and thermal performance. The geothermal system efficiently operates by circulating the working fluid (which is pure water) from the space between the two heat exchanger pipes into the well, allowing it to absorb heat from the well formations and the bottom of the well, thus transforming it into hot fluid. The hot geothermal working fluid is confidently returned to the wellhead under high pressure through the internal pipe of the CBHE. However, due to the long length of the well, there is a temperature drop in the geofluid's return path to the wellhead. Using thermal insulation can prevent or minimize temperature drop in the CBHE by maintaining fluid temperature and avoiding heat loss around the internal pipe. So, the CBHE is the ideal choice for utilizing AOW. With proper insulation, the system can deliver efficient and effective performance.

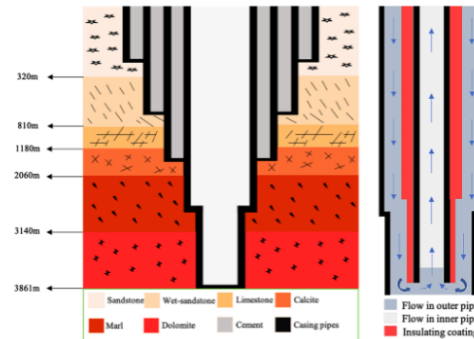


Fig. 2. The schematic of the Ahwaz AOW and the designed CBHE [22]

## 2.2 Kalina Cycle System 11 (KC-11)

The KC-11 is an advanced thermodynamic process that utilizes a binary mixture, typically water and ammonia, as the working fluid to improve the efficiency of power generation systems. The fundamental principle behind the KC-11 is its ability to exploit the non-isothermal boiling and condensation characteristics of the binary mixture, which allows for more effective heat absorption and rejection compared to traditional RC that use a single-component fluid like water. The KC-11 finds its main application in waste heat recovery and geothermal power plants due to its ability to operate at lower temperatures, making it more efficient in converting low-grade heat sources into electricity. It is known for its higher thermal efficiency when compared to the RC, particularly in applications where the heat source is available at varying temperatures. The thermodynamics of the KC-11 involves mass and energy balances, as well as the behavior of the ammonia-water mixture. Some of the most important equations related to the cycle are as follows:

### 2.2.1 First Law of Thermodynamics for a Control Volume

The energy balance across any control volume (like a turbine, heat exchanger, or separator) is governed by the steady-state version of the First Law of Thermodynamics:

$$\dot{Q} - \dot{W} = \sum \dot{m}_{out} \dot{h}_{out} - \sum \dot{m}_{in} \dot{h}_{in} \quad (1)$$

Where:

- $\dot{Q}$  is the heat transfer rate to/from the control volume.
- $\dot{W}$  is the work done by the turbine.
- $\dot{m}$  is the mass flow rate.
- $\dot{h}$  are the specific enthalpies of the incoming and outgoing streams.

### 2.2.2 Mixture Properties

The specific enthalpy of the binary ammonia-water mixture varies with both pressure and composition. For any stream, the enthalpy is:

$$h_{mix} = x_{NH_3} h_{NH_3} + (1 - x_{NH_3}) h_{H_2O} \quad (2)$$

Where  $x_{NH_3}$  is the ammonia mass fraction, and  $h_{NH_3}$ ,  $h_{H_2O}$  are the specific enthalpies of pure ammonia and water, respectively.

### 2.2.3 Turbine Work

In the expansion process through the turbine, the work output is given by:

$$W_{turbine} = \dot{m}(h_{in} - h_{out}) \quad (3)$$



Where  $h_{in}$  and  $h_{out}$  are the specific enthalpies at the inlet and outlet of the turbine.

#### 2.2.4 Heat Exchanger Energy Balance

In heat exchangers, the energy balance can be written as:

$$Q_{in} = \dot{m}(h_{in} - h_{out}) \quad (4)$$

This represents the heat absorbed or rejected by the working fluid in heat exchangers.

#### 2.2.5 Ammonia Separation

A distinctive part of the KC-11 is the separator, where a high-pressure stream is separated into a vapor phase rich in ammonia and a liquid phase rich in water. The energy balance for the separator is given by:

$$\dot{m}_{in}h_{in} = \dot{m}_{vapor}h_{vapor} + \dot{m}_{liquid}h_{liquid} \quad (5)$$

Where  $h_{in}$ ,  $h_{vapor}$ , and  $h_{liquid}$  are the specific enthalpies of the inlet, vapor, and liquid streams, respectively.

### 2.3 RO Desalination System

RO is a widely used water purification process that removes dissolved salts and impurities from water by applying pressure to push water through a semipermeable membrane. The membrane allows water molecules to pass but blocks larger particles, including salts, bacteria, and other contaminants. RO is used in various applications, including desalination of seawater, wastewater treatment, and production of ultrapure water for industries and households. In an RO system, the driving force is the pressure applied to the feed water, which must be greater than the natural osmotic pressure to reverse the flow of water through the membrane. This process separates the feed water into two streams: the permeate and the concentrate.

#### 2.3.1 Osmotic Pressure

The osmotic pressure  $\Pi$  of a solution, which depends on the concentration of solutes, is given by:

$$\Pi = iMRT \quad (6)$$

Where:

- $i$  is the van 't Hoff factor (number of particles into which a solute dissociates),
- $M$  is the molar concentration of the solute (mol/L),
- $R$  is the universal gas constant (0.0821 L·atm/mol·K),
- $T$  is the absolute temperature in Kelvin.

#### 2.3.2 Permeate Flux

The rate of water flow through the membrane, also called the permeate flux, is described by:

$$J = A(P - \Delta\Pi) \quad (7)$$

Where  $J$  is the permeate flux (volume of water per membrane area per time, typically measured in L/m<sup>2</sup>/h),  $A$  is the membrane's water permeability coefficient,  $P$  is the applied pressure,  $\Delta\Pi$  is the difference in osmotic pressure across the membrane.

#### 2.3.3 Salt Rejection

The effectiveness of the RO membrane in removing dissolved salts is measured by the salt rejection rate, which is calculated as:



$$R = \left(1 - \frac{C_{\text{permeate}}}{C_{\text{feed}}}\right) \times 100 \quad (8)$$

Where:

- $C_{\text{permeate}}$  is the salt concentration in the permeate stream,
- $C_{\text{feed}}$  is the salt concentration in the feed stream.

#### 2.3.4 Recovery Rate

The recovery rate is the proportion of feed water that is converted into permeate:

$$Y = \frac{Q_{\text{permeate}}}{Q_{\text{feed}}} \times 100 \quad (9)$$

Where  $Q_{\text{permeate}}$  is the volumetric flow rate of permeate, and  $Q_{\text{feed}}$  is the volumetric flow rate of the feed water.

### 3. RESULTS AND DISCUSSION

#### 3.1 KC-11 Section

The proposed KC-11 system utilizes a water-ammonia mixture as the working fluid, enhancing efficiency by leveraging the unique thermodynamic properties of this binary mixture. The schematic diagram of the proposed KC-11 cycle is presented in Figure 3.

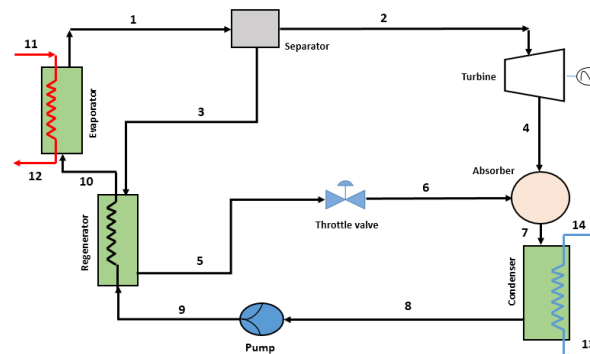


Fig. 3. Schematic diagram of the proposed KC-11 system

The process starts as the water-ammonia mixture is heated in the evaporator (11), where an external geothermal heat source from the proposed AOW transfers heat to the mixture. This causes partial evaporation, creating a two-phase mixture. The mixture then flows into the separator, where it is divided into a high-ammonia vapor and a low-ammonia liquid. This separation enables more effective use of the working fluid in the power generation process. Subsequently, the high-ammonia vapor from the separator enters the turbine, expanding and generating power. Thus, high-energy vapor drives the turbine (4), which is coupled to a generator, converting thermal energy into electrical power. The low-ammonia liquid from the separator is routed through a throttle valve (6), reducing its pressure. After that, this low-pressure liquid enters the absorber (7), where it absorbs the vapor from the turbine exhaust, forming a rich water-ammonia solution. The combined mixture from the absorber flows into the condenser (13), where it releases heat to the cooling water, causing it to condense fully into a liquid phase. Next, the liquid solution is pumped (8) to a higher pressure and pre-heated in the regenerator (10), where it absorbs heat from the fluid exiting the evaporator. As a result, this regenerative heating step improves the overall cycle efficiency. The pre-heated fluid is sent back to the evaporator to restart the cycle.

There are these three main assumptions for this model:

- The system assumes no heat loss and no pressure drops within pipes and heat exchangers.



- The system's maximum pressure is set at 3 MPa.
- Any exergy destruction in the cooling water stream is considered negligible.

Table 1 presents the operational conditions for the cycle.

**Table 1.** Operational conditions of the KC-11 system

Parameter	Value
$\dot{m}_{11}$ (kg/s)	9
$\dot{m}_{13}$ (kg/s)	1
$T_{11}$ (K)	378
$T_{12}$ (K)	343
$T_{13}$ (K)	290
$T_0$ (K)	300
$\eta_{turbine}$ (%)	80
$\eta_{pump}$ (%)	80

### 3.1.1 First Law Analysis:

In this system, the heat source is a geothermal well that provides the required heat for the power generation cycle via a geothermal fluid. The heat input to the system is obtained from the following equation:

$$Q_{in} = \dot{m}_h c_h (T_{11} - T_{12}) \quad (10)$$

Where  $Q_{in}$  is defined as heat input to the system,  $\dot{m}_h$  and  $c_h$  are defined as the mass flow rate and specific heat capacity of geothermal working fluid, respectively, and  $T_{11}$  and  $T_{12}$  indicates the temperature of geothermal working fluid at the inlet and outlet of the evaporator, respectively.

### 3.1.2 Turbine Work Output and Cycle Efficiency:

Calculations for expansion turbine work output and cycle efficiency. are based on the first law of thermodynamics, using the following equations:

$$w = \dot{m}_2 (h_2 - h_4) \quad (11)$$

$$\eta = \frac{w}{Q_{in}} \quad (12)$$

Where  $w$  is defined as the turbine work output,  $\dot{m}_2$  indicates mass flow rate of ammonia-water entering the turbine,  $h_2$  and  $h_4$  are the enthalpy of ammonia-water at the inlet and outlet of turbine, respectively. Also,  $\eta$  presents cycle efficiency.

### 3.1.3 Exergy Analysis of the Cycle:

In this system,  $E_{in}$  and  $E_{out}$  represent the exergy of the proposed AOW heat source at the inlet and outlet of the evaporator, respectively.  $T_{11}$ ,  $T_{12}$ , and  $T_0$  correspond to the inlet and outlet temperatures of the geothermal working fluid in the evaporator and reference temperature, respectively.

$$E_{in} = \dot{m}_h c_h (T_{11} - T_0 - (T_0 \ln \frac{T_{11}}{T_0})) \quad (13)$$

$$E_{out} = \dot{m}_h c_h (T_{12} - T_0 - (T_0 \ln \frac{T_{12}}{T_0})) \quad (14)$$

$$\eta_{exergy} = \frac{w}{E_{in}} \quad (15)$$

As seen in the graphs in Figure 4, the trend of parameter variations relative to the working fluid composition is quite similar across all cases. When ammonia-water pressure at the evaporator outlet is 15 bar,



thermal efficiency peaks at a lower ammonia concentration with a sharper decline beyond this peak. In contrast, the 20-bar cycle achieves a broader, more stable efficiency curve, suggesting that higher pressure may enhance efficiency over a wider concentration range. Also, the 20-bar condition yields a higher maximum work output and maintains it over a wider concentration range, whereas the 15-bar condition shows a narrower peak. The 20-bar pressure setting is preferable for geothermal applications, as it not only provides a higher work output but also sustains efficiency across a broader range of ammonia concentrations. This flexibility makes it better suited for the variable conditions typical of geothermal heat sources, maximizing performance and adaptability.

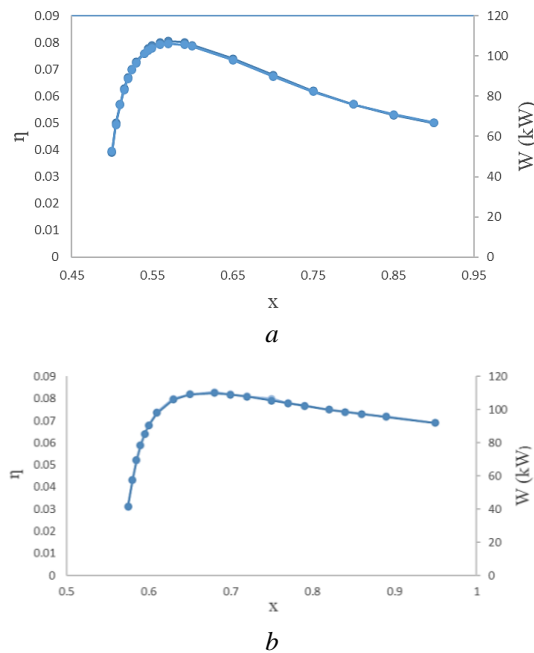


**Fig. 4.** Work output and thermal efficiency as a function of ammonia-water concentration at the evaporator outlet for a) 15 bar and b) 20 bar ammonia-water pressure

Figure 5 shows that the exergy efficiency exhibits a peak value at an intermediate ammonia-water concentration for both pressure conditions. For the 20-bar cycle, the peak exergy efficiency is around 0.33, occurring at a concentration of approximately 0.65-0.70. In contrast, the 15-bar cycle exhibits a slightly lower peak exergy efficiency of around 0.32, at a concentration of 0.55-0.60. While the difference in peak exergy efficiency between the two pressure conditions is relatively small (0.33 vs 0.32), other factors may favor the selection of the 20-bar operating pressure. Higher operating pressures generally allow for more compact and cost-effective heat exchangers, as the higher pressure reduces the required heat transfer area. Additionally, higher pressure cycles can often achieve better volumetric efficiency, leading to more compact and potentially less expensive turbomachinery. Furthermore, the exergy efficiency curve for the 20-bar cycle is broader and flatter compared to the 15-bar case. This suggests that the 20-bar cycle may be more tolerant to variations in operating conditions and composition changes, potentially simplifying the control and operation of the power plant. Considering the marginally higher peak exergy efficiency, the potential advantages in the heat exchanger and turbomachinery design, and the broader operational flexibility, the 20-bar operating pressure may be the preferred choice for this KC-11 application utilizing geothermal heat as the energy source.

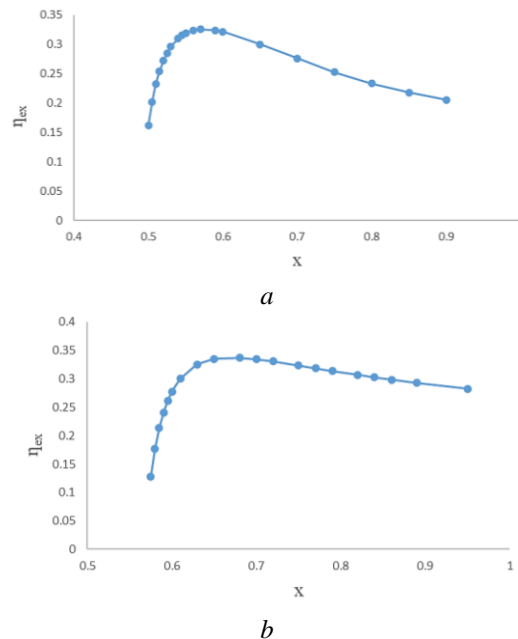


**Fig. 5.** Exergy efficiency as a function of ammonia-water concentration at the evaporator outlet for a) 15 bar and b) 20 bar ammonia-water pressure

To verify the results., it is essential to understand the roles of temperature and mass flow rate of the geothermal working fluid in the evaporator of the KC-11 cycle. Both of these factors significantly influence the net electricity output. As the geothermal working fluid temperature increases, it enhances the vaporization process, resulting in higher turbine power output and ultimately boosting the system's net electricity production. Similarly, a higher mass flow rate allows for a greater amount of heat to be transferred to the working fluid in the evaporator. This increased heat input elevates the pressure and temperature levels in the system, which contributes to better turbine performance and higher electricity generation. Noorollahi et al. [27] demonstrated that in Case DQ when the exit fluid temperature of the geothermal fluid was 145.7 °C and its mass flow rate was 4.875 kg/s, the electricity production reached 111.7 kW. However, a slight decrease in temperature to 137.8 °C, along with an increase in mass flow rate to 11.9 kg/s, resulted in a significant rise in electricity production. Table 2 compares the results of this study with those of previous research.

**Table 2.** The comparison of obtained result in the present study and other studies

Case	Bottom-hole temperature (°C)	Outlet temperature (°C)	Flow rate (kg/s)	Net power (kWh)
Present study	138.7	104.1	9.05	110
DQ-I [27]	159.8	145.7	4.875	111.7
DQ-II [27]	159.8	137.8	11.9	364
Bu et al. [29]	195	129.8	1.54	53.7
Cheng et al. [30]	255	136.1	0.18	154

### 3.2 RO Section

In the context of seawater desalination, the RO system is employed. An industrial unit has requested the production of 806 m<sup>3</sup>/day of freshwater with a recovery rate of 55%. The specifications of the feed and desired permeate can be found in Table 3 below.



**Table 3.** specification of the proposed RO system

Specifications	Value
Feedwater TDS (mg/l)	35000
Feedwater temperature (°C)	25
Permeate flow rate (m <sup>3</sup> /day)	806
Permeate pH	7
Recovery rate	55%
Silt Density Index (SDI)	<3
Flux (LMH)	13-17
Membrane Active area (m <sup>2</sup> )	37

It is important to highlight that a recovery rate of 55% for a seawater system is considered relatively high, as these systems typically operate at around 30%. Therefore, a single-stage system will not satisfy the client's desired outcomes; instead, a two-stage RO system should be contemplated, as depicted in Figure 6.

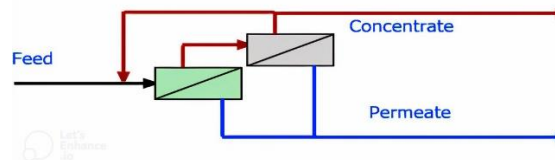


**Fig. 6.** Schematic diagram of the proposed two-stage RO system

To minimize capital costs, it is crucial to limit the number of membranes. However, to optimize operational costs, maximizing the number of membranes is necessary. An additional benefit is that increasing the system's recovery rate will naturally lower expenses. Therefore, the initial step is to accurately calculate the number of membranes and pressure vessels using the following equation:

$$N_{\text{membrane}} = \frac{Q_p}{(\text{Flux}) \times (S_E)} \quad (16)$$

In this context,  $N_{\text{membrane}}$  is defined as the total number of membranes calculated,  $Q_p$  represents the flow rate of permeate (measured in L/hr), Flux denotes the designed flux of the system (expressed in liters per square meter per hour, or LMH), and  $S_E$  indicates the active membrane area (m<sup>2</sup>). It is essential to recognize that the range for the designed flux of the proposed RO system, typically between 13 and 17 LMH in this instance, is contingent upon the characteristics of the feedwater, seawater in this case, and the SDI of the feedwater. Consequently, if the designed flux is set at the minimum value, the calculated number of membranes will reach its maximum. Conversely, if the designed flux is established at the maximum value, the calculated number of membranes will be at its minimum. Therefore, the number of pressure vessels required for the system must be determined using the following equation:

$$N_{pv} = \frac{N_{\text{membrane}}}{C_{pv}} \quad (17)$$

Where:

- $N_{pv}$  represents the number of calculated pressure vessels.
- $C_{pv}$  denotes the capacity of each pressure vessel.

Upon determining the total number of membranes required for the pressure vessels, it is essential to recognize that, given a recovery rate of 55%, a single-stage RO system is impractical. Consequently, the RO system should operate in two stages. It is vital to specify how many pressure vessels are needed for each stage. This is defined by the ratio between the stages, which can be calculated using the following equation:



$$R = \left[ \frac{1}{(1-Y)} \right]^{\frac{1}{n}} \quad (18)$$

Where  $R$  is the ratio of stages,  $Y$  is the recovery rate, and  $n$  is the number of stages. The equation below will determine the number of pressure vessels needed for each stage. To accurately ascertain the number of pressure vessels required in stage two, one should commence with  $N_{pv(1)}$ , which represents the count established in stage one. Upon determination of this value, the simulation will be executed promptly.

$$N_{pv(1)} = \frac{N_{pv}}{1+R^{-1}} \quad (19)$$

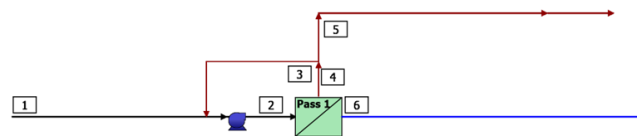
Here is a summary of the calculated parameters, as presented in Table 4. It is valuable to recognize that a slight difference may exist between the calculated values and the optimal values required to meet expectations. This insight can guide improvements and enhance overall accuracy in our measurements.

**Table 4.** Calculated parameters for the simulation

Parameter	Value
$N_{membrane}$	72
$C_{pv}$	6
$R$	1.5
$N_{pv(1)}$	7
$N_{pv(2)}$	5

### 3.2.1 RO System Overview

Based on the input parameters and computed data, the software run yielded results as summarized as below:



#	Description	Flow (m <sup>3</sup> /d)	TDS (mg/L)	Pressure (bar)		
1	Raw Feed to RO System	1,464	35,000	0.0		
2	Net Feed to Pass 1	1,614	39,158	68.4		
3	Concentrate Recycle from Pass 1 to Pass 1	154.3	77,550	65.2		
4	Total Concentrate from Pass 1	811.9	77,551	65.2		
5	Net Concentrate from RO System	657.6	77,551	65.2		
6	Net Product from RO System	805.1	282.5	0.0		
Total # of Trains		1	Online = 1	Standby = 0	RO Recovery	55.0 %
System Flow Rate		(m <sup>3</sup> /d)	Net Feed = 1,464	Net Product = 805.1		

Pass	Pass 1
Stream Name	Stream 1
Water Type	Sea Water (Conventional pretreatment, SDI<3)
Number of Elements	72
Total Active Area	(m <sup>2</sup> ) 2676



Feed Flow per Pass	(m <sup>3</sup> /d)	1,614
Feed TDS <sup>a</sup>	(mg/L)	39,158
Feed Pressure	(bar)	68.4
Flow Factor Per Stage		1.00, 1.00
Permeate Flow per Pass	(m <sup>3</sup> /d)	805.1
Pass Average flux	(LMH)	12.5
Permeate TDS <sup>a</sup>	(mg/L)	282.5
Pass Recovery		49.9 %
Average NDP	(bar)	16.2
Specific Energy	(kWh/m <sup>3</sup> )	4.78
Temperature	(°C)	25.0
pH		6.9
Chemical Dose		-
RO System Recovery		55.0 %
Net RO System Recovery		55.0%

Stage	Elements	#PV	#Els per PV	Feed				Concentrate			Permeate			
				Feed Flow	Recirc Flow	Feed Press	Boost Press	Conc Flow	Conc Press	Press Drop	Perm Flow	Avg Flux	Perm Press	Perm TDS
				(m <sup>3</sup> /d)	(m <sup>3</sup> /d)	(bar)	(bar)	(m <sup>3</sup> /d)	(bar)	(bar)	(m <sup>3</sup> /d)	(LMH)	(bar)	(mg/L)
1	SW30HRLE-400	7	6	1,614	154.3	68.0	0.0	909.0	66.7	1.3	707.5	18.9	0.0	173.0
2	SW30HRLE-400	5	6	909.0	0.0	66.5	0.0	811.9	65.2	1.4	97.6	3.6	0.0	1,077

As shown, after achieving optimal conditions for this problem, the required potable water production target of approximately 806 m<sup>3</sup>/day (practically reaching 805.1 m<sup>3</sup>/day) necessitated a feed water flow rate of 1464 m<sup>3</sup>/day. To attain this output, the system's operational pressure stabilized at 68.4 bar, a value within acceptable limits compared to the initial operational conditions specified. It is noteworthy that the initial TDS concentration of the feed water was recorded at 35,000 mg/L, which increased to 39,158 mg/L upon incorporating a return flow into the feed. However, the system effectively reduced the TDS level to a favorable 282.5 mg/L, demonstrating that this desalination system, with a 55% recovery rate and a two-stage process, successfully converts seawater into potable water. A critical metric observed in these results is the specific energy consumption, indicating that this desalination system requires 4.78 kWh of energy per 1 m<sup>3</sup> of potable water produced. This energy demand is efficiently met by the KC-11. Additionally, the pH level of the feed water was measured at 6.9, maintaining appropriate conditions for the desalination process. Also, the two-stage RO system modeled in WAVE software uses SW30HRLE-400 elements, with a feed flow of 1,614 m<sup>3</sup>/day at 68.0 bar in Stage 1, dropping to 909.0 m<sup>3</sup>/day at 66.5 bar in Stage 2. Stage 1 produces a permeate of 707.5 m<sup>3</sup>/day with a low TDS of 173 mg/L and high flux (18.9 LMH), demonstrating effective salt rejection. However, permeate flow decreases to 97.6 m<sup>3</sup>/day in Stage 2, with TDS rising to 1,077 mg/L and flux lowering to 3.6 LMH, reflecting the challenges of increased feed concentration and osmotic pressure in the second stage. This setup highlights the trade-off between recovery and permeate quality, with Stage 1 achieving higher efficiency, while Stage 2 experiences diminished quality due to concentration effects.

Table 5 has been included to validate the outcomes derived from the RO system. Noorollahi et al. [28] utilized a 12-effect MED system powered by geothermal energy to meet its heating requirements. The overall specifications of the desalination systems are outlined in the table below. The findings indicated that this system can produce a daily output of 600 m<sup>3</sup> of potable water from 13.4 kg/s of seawater. Subsequently, Norouzi et al. [22] improved MED system by integrating flash boxes and implementing brine recovery across all effects. This



3rd International Congress for  
**Chemical Engineering and  
Petroleum Industry students**

[www.cco.cdsts.ir](http://www.cco.cdsts.ir)



سومین کنگره بین‌المللی  
**دانشجویان مهندسی  
شیمی و صنعت نفت**

modification resulted in a significant increase in freshwater production, raising output from 600 m<sup>3</sup>/day to 806 m<sup>3</sup>/day, which highlights the substantial impact of flash boxes and brine recovery.

**Table 5.** The comparison of fresh water production in the present study and previous studies

Case	Desalination System	Feed water	TDS	Drinkable water
Present study	RO (with recycle)	17 kg/s	35000 mg/L	805.1 m <sup>3</sup> /day
Noorollahi et al. [27]	MED	13.4 kg/s	35000 mg/L	600 m <sup>3</sup> /day
Norouzi et al. [22]	Modified MED	13.4 kg/s	35000 mg/L	806 m <sup>3</sup> /day



3rd International Congress for  
**Chemical Engineering and  
Petroleum Industry students**



سومین کنگره بین‌المللی  
**دانشجویان مهندسی  
شیمی و صنعت نفت**

[www.cco.cdsts.ir](http://www.cco.cdsts.ir)

#### 4. CONCLUSION

*In conclusion, this study has successfully demonstrated the feasibility and efficiency of a combined KC-11 power generation and RO desalination system, utilizing an AOW as an external heat source. Through the use of EES software for KC-11 simulation, it was observed that the system could generate power efficiently at both 15-bar and 20-bar pressures, yielding outputs of approximately 106 kWh and 110 kWh, respectively. The exergy analysis further revealed that operating at higher pressures, such as 20-bar, not only enhances volumetric efficiency but also offers operational resilience. This higher-pressure cycle is more compact and potentially more economical, making it an attractive solution for power generation from low-grade thermal sources. For desalination, a two-stage RO system was simulated using Wave software, focusing on achieving a balance between high water recovery and operational cost efficiency. With a recovery rate of 55% and optimized with 72 membrane elements, the RO system demonstrated the capacity to produce 805.1 m<sup>3</sup>/day of potable water with a TDS level of 282.5 mg/L—substantially lower than that of the feedwater. Furthermore, the system's specific energy consumption of 4.78 kW per 1 m<sup>3</sup> indicates a promising pathway for energy-efficient desalination. This research not only underscores the potential for integrating waste-heat power generation with desalination but also highlights the importance of system optimization for sustainable and cost-effective operation. The findings point toward a viable model for utilizing AOW energy resources to meet both power and freshwater demands, with potential applications in regions where energy efficiency and resource conservation are paramount.*



## 5. REFERENCES

- [1] Bundschuh, J., et al., *State-of-the-art of renewable energy sources used in water desalination: Present and future prospects*. *Desalination*, 2021. 508: p. 115035.
- [2] Kheirinejad, S., et al., *The effect of reducing per capita water and energy uses on renewable water resources in the water, food and energy nexus*. *Scientific Reports*, 2022. 12(1): p. 7582.
- [3] Panagopoulos, A., *Water-energy nexus: desalination technologies and renewable energy sources*. *Environmental Science and Pollution Research*, 2021. 28(17): p. 21009-21022.
- [4] Sedayevatan, S., et al., *Uncertainty Covered Techno-Enviro-Economic Viability Evaluation of a Solar Still Water Desalination Unit Using Monte Carlo Approach*. *Energies*, 2023. 16(19): p. 6924.
- [5] Sohani, A., et al., *An optimum energy, economic, and environmental design based on DEVAP concept to reach maximum heat recovery in a PV-wind turbine system with hydrogen storage*. *Energy Conversion and Management*, 2023. 288: p. 117147.
- [6] Sohani, A., et al., *Determination of the best air space value for installation of a PV façade technology based on 4E characteristics*. *Energy*, 2023. 262: p. 125386.
- [7] Sharmin, T., et al., *A state-of-the-art review on geothermal energy extraction, utilization, and improvement strategies: conventional, hybridized, and enhanced geothermal systems*. *International Journal of Thermofluids*, 2023. 18: p. 100323.
- [8] Lund, J.W. and A.N. Toth, *Direct utilization of geothermal energy 2020 worldwide review*. *Geothermics*, 2021. 90: p. 101915.
- [9] Hu, Y., H. Cheng, and S. Tao, *Opportunity and challenges in large-scale geothermal energy exploitation in China*. *Critical Reviews in Environmental Science and Technology*, 2022. 52(21): p. 3813-3834.
- [10] Gong, F., et al., *Evaluation of geothermal energy extraction in Enhanced Geothermal System (EGS) with multiple fracturing horizontal wells (MFHW)*. *Renewable Energy*, 2020. 151: p. 1339-1351.
- [11] Sohani, A., et al., *Thermography and machine learning combination for comprehensive analysis of transient response of a photovoltaic module to water cooling*. *Renewable Energy*, 2023. 210: p. 451-461.
- [12] Sohani, A., et al., *Building integrated photovoltaic/thermal technologies in Middle Eastern and North African countries: Current trends and future perspectives*. *Renewable and Sustainable Energy Reviews*, 2023. 182: p. 113370.
- [13] Tester, J.W., et al., *The evolving role of geothermal energy for decarbonizing the United States*. *Energy & environmental science*, 2021. 14(12): p. 6211-6241.
- [14] Kalogirou, S.A., *Introduction to renewable energy powered desalination*, in *Renewable energy powered desalination handbook*. 2018, Elsevier. p. 3-46.
- [15] Sohani, A., et al., *Techno-economic evaluation of a hybrid photovoltaic system with hot/cold water storage for poly-generation in a residential building*. *Applied Energy*, 2023. 331: p. 120391.
- [16] Santos, L., A.D. Taleghani, and D. Elsworth, *Repurposing abandoned wells for geothermal energy: Current status and future prospects*. *Renewable Energy*, 2022. 194: p. 1288-1302.
- [17] Kurnia, J.C., et al., *Geothermal energy extraction using abandoned oil and gas wells: Techno-economic and policy review*. *International Journal of Energy Research*, 2022. 46(1): p. 28-60.
- [18] Harris, B., M. Lightstone, and S. Reitsma, *A numerical investigation into the use of directionally drilled wells for the extraction of geothermal energy from abandoned oil and gas wells*. *Geothermics*, 2021. 90: p. 101994.
- [19] Ebrahimi, D., et al., *A brief survey on case studies in geothermal energy extraction from abandoned wells*, in *Utilization of Thermal Potential of Abandoned Wells*. 2022, Elsevier. p. 75-96.
- [20] Liu, Z., et al., *Research progress of technologies and numerical simulations in exploiting geothermal energy from abandoned wells: a review*. *Geoenergy Science and Engineering*, 2023. 224: p. 211624.
- [21] Ashena, R., *Analysis of some case studies and a recommended idea for geothermal energy production from retrofitted abandoned oil and gas wells*. *Geothermics*, 2023. 108: p. 102634.
- [22] Norouzi, M., et al., *CuO/water and Al<sub>2</sub>O<sub>3</sub>/water nanofluids as working fluid in an abandoned oil well to improve thermal performance in the seawater desalination process*. *Journal of the Taiwan Institute of Chemical Engineers*, 2023. 144: p. 104754.



3rd International Congress for  
**Chemical Engineering and  
Petroleum Industry students**



سومین کنگره بین‌المللی  
**دانشجویان مهندسی  
شیمی و صنعت نفت**

[www.cco.cdsts.ir](http://www.cco.cdsts.ir)

- [23] Rezaie, K., et al., *Solar-driven chemisorption cogeneration system integrated with thermal energy storage. Journal of Energy Storage*, 2024. 76: p. 109705.
- [24] Akbari, M., et al., *Energy and exergy analyses of a new combined cycle for producing electricity and desalinated water using geothermal energy. Sustainability*, 2014. 6(4): p. 1796-1820.
- [25] Bai, H., et al., *Development of a novel power and freshwater cogeneration plant driven by hybrid geothermal and biomass energy. Case Studies in Thermal Engineering*, 2023. 52: p. 103695.
- [26] Alirahmi, S.M., et al., *Multi-objective design optimization of a multi-generation energy system based on geothermal and solar energy. Energy Conversion and Management*, 2020. 205: p. 112426.
- [27] Noorollahi, Y., et al., *Numerical simulation of power production from abandoned oil wells in Ahwaz oil field in southern Iran. Geothermics*, 2015. 55: p. 16-23.
- [28] Noorollahi, Y., S. Taghipoor, and B. Sajadi, *Geothermal sea water desalination system (GSWDS) using abandoned oil/gas wells. Geothermics*, 2017. 67: p. 66-75.
- [29] Bu, X., W. Ma, and H. Li, *Geothermal energy production utilizing abandoned oil and gas wells. Renewable energy*, 2012. 41: p. 80-85.
- [30] Cheng, W.-L., et al., *Studies on geothermal power generation using abandoned oil wells. Energy*, 2013. 59: p. 248-254.